Eur. Phys. J. A **8**, 501–510 (2000)

THE EUROPEAN PHYSICAL JOURNAL A

One- and two-neutron transfer reactions on ^{12}C with the weakly bound ^{6}He projectile

I.V. Krouglov[2,3,a] and W. von Oertzen[1,2,b]

[1] Freie Universität Berlin, Fachbereich Physik, Arnimallee 14, 14195 Berlin, Germany
[2] Hahn-Meitner-Institut Berlin, Glienicker Strasse 100, 14109 Berlin, Germany
[3] St. Petersburg State University, Nuclear Physics Department, Uljanovskaja str. 1, 198904 St. Petersburg, Russia

Received: 13 June 2000
Communicated by D. Schwalm

Abstract. Using the framework of the coupled reaction channels (CRC) the one- and two-neutron transfer process initiated by the weakly bound nucleus ^{6}He on ^{12}C at an energy of $E_L = 5.9$ MeV is studied. The absolute cross-sections for a few states in ^{14}C are well reproduced within a factor 2 in second order, using microscopic wave functions of ^{6}He and ^{12}C. Only a small dependence of the cross-section on details of the ^{6}He wave function is observed. Good fits to the data are obtained in a calculation with full coupling (25 iterations) with renormalised optical potential parameters and spectroscopic amplitudes of ^{6}He.

PACS. 25.70.-z Low and intermediate energy heavy-ion reactions – 25.60.Je Transfer reactions – 25.10.+s Nuclear involving few-nucleon systems

1 Introduction

Reactions induced by ^{6}He have attracted great attention [1,2] because of its unusual structural properties related to the fact that the odd isotope ^{5}He is unbound. The ^{6}He$_{0^+}$ ground state is an example of a three-body bound state or "Borromean" nucleus, because the subunits of two particles are unbound, with the three-body system forming a bound system. Apart of break-up reactions yielding spectroscopic information on the neutron configurations in the ^{6}He$_{0^+}$ ground state, the two-neutron transfer has recently been studied experimentally [3,4], for example also in the α+^{6}He elastic transfer channel [5,6].

The study of two-neutron transfer induced by heavy ions has a long history [7,8,10]; there has been considerable progress in the theoretical description of the two-nucleon transfer over the last two decades in particular in attempts to reproduce absolute cross-sections. The enhanced transfer of nucleon pairs, in particular of two neutrons has attracted large interest due to its relation to pairing correlations. In a microscopic basis it has been treated on the basis of mixed shell model wave functions with great success [8,9]. With modern computational techniques and using the coupled reaction channel (CRC) approaches [11], it became possible to get satisfactory reproduction of the absolute cross-sections as well as of the shapes of differential cross-sections [9,10]. The advent of radioactive beams now allows the study of two-neutron transfer reactions induced by weakly bound nuclei. Among the lighter nuclei, the ^{6}He-nucleus has been available for some time, and data on two-neutron transfer have become available recently.

In the present study we report on an analysis of one- and two-neutron transfer reaction induced by ^{6}He on a ^{12}C target related to the experimental results of ref. [3]. The incident energy of $E_{\rm lab} = 5.9$ MeV is above the Coulomb barrier, and differential cross-sections for individual states in ^{14}C have been reported, as well as for the elastic channel. For the structure of ^{14}C there are several studies, in particular for the structure of the 0^+ states (ground state and at 6.5 MeV excitation) the configuration mixing between the *p*-shell and the *sd*-shell has been discussed [12,13]. With the CRC methods implemented in the code FRESCO [11] we have good conditions to make state-of-the-art calculations and compare with the recent experimental result.

2 Coupled Reaction Channel calculations

The main aim of the present study is to test the dynamical and structural properties of the ^{6}He-induced reactions. For a better understanding it is of importance to have a look at the Q-values of the one- and two-neutron transfer channels. We show in fig. 1 the relevant quantities for the ^{5}He and ^{4}He channels. Q-values tend to be rather positive due to the comparably weak binding of the neutrons in ^{6}He. Inspecting fig. 1 we recognise that the one-neutron

[a] e-mail: kruglov@nuclpc1.phys.spbu.ru
[b] e-mail: oertzen@hmi.de

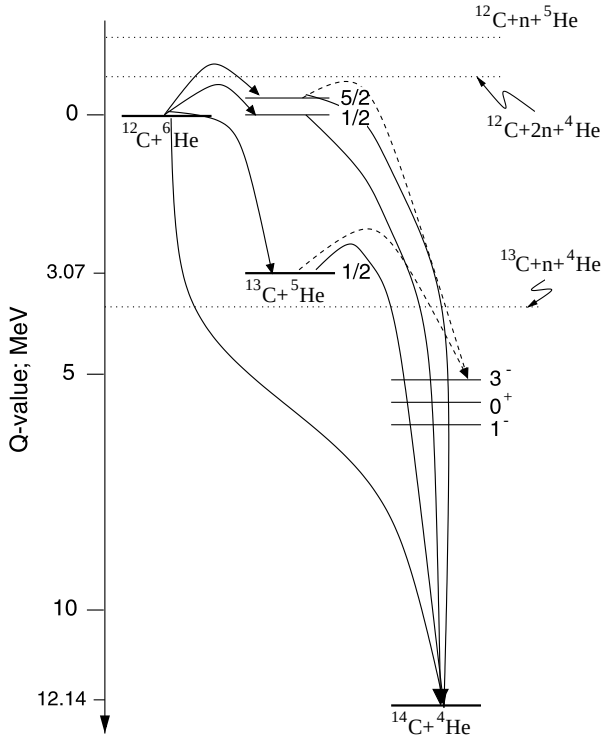

Fig. 1. Q-value diagram for one and two-neutron transfer in the system ^{6}He + ^{12}C. The Q-value for the ^{14}C ground state is very positive and introduces a mismatch. For some transitions one- and two-step processes are indicated.

transfer has moderately positive Q-values, whereas the Q-value for the ground state of ^{14}C reaches up to 12 MeV. The one-step and two-step two-neutron transfer routes are drawn for illustration. For the excited states in ^{14}C the individual steps in the two-neutron transfers are rather similar, whereas the second energy step for the ground-state (GS) transition of ^{14}C is large as compared to the first one.

A particular feature is that in one neutron transfers the ground state of the ^{5}He nucleus a $p_{3/2}$ resonance at 0.89 MeV with a width of 600 keV is formed, and therefore no data can be made available for the one-neutron transfer cross-section in these studies.

2.1 Basic formulae for the one- and two-nucleon transfer

In the present work the two-particle transfer has been calculated using the "standard" procedure, the transfer process is treated in the coupled reaction channel scheme [11], where single-neutron and two-neutron transfer are treated in a consistent way. The matrix elements for the one-nucleon transfer are defined in the usual way by the overlap of the single-particle wave functions $\langle \Phi_{^4\mathrm{He}} | \Phi_{^5\mathrm{He}} \rangle = \phi_{1i}(r_i)$ for the ^{5}He overlap and $\langle \Phi_{^{13}\mathrm{C}} | \Phi_{^{12}\mathrm{C}} \rangle = \phi_{1f}(r_f)$ for the overlap of ^{12}C with ^{13}C. The relevant spectroscopic amplitudes and quantum numbers for the single-nucleon states in carbon are given in table 1 and for two nucleons

Table 1. Spectroscopic amplitudes for wave functions in C-isotopes.

J^π for $\langle {}^{13}\mathrm{C}_{J^\pi} \vert {}^{12}\mathrm{C}_{\mathrm{gs}} \rangle$	ref. [16]	This work
1/2-	0.88	0.77
1/2+	0.81	0.77
5/2+	0.76	0.77
J^π for $\langle {}^{14}\mathrm{C}_{J^\pi} \vert {}^{13}\mathrm{C}_{1/2^-} \rangle$	ref. [19]	This work
0^+	1.35	1.16
1^-		1.00
0^+		0.56
3^-		1.00
J^π for $\langle {}^{14}\mathrm{C}_{J^\pi} \vert {}^{13}\mathrm{C}_{1/2^+} \rangle$	ref. [19]	This work
0^+	0.17	0.17
1^-		1.00
0^+		0.60
J^π for $\langle {}^{14}\mathrm{C}_{J^\pi} \vert {}^{13}\mathrm{C}_{5/2^+} \rangle$	ref. [19]	This work
0^+	0.38	0.51
0^+		0.97
3^-		1.00

Table 2. Two-nucleon amplitudes for the configurations of ^{14}C states.

Overlap	$(p_{\frac{1}{2}})^2$	$(s_{\frac{1}{2}})^2$	$(d_{\frac{5}{2}})^2$	Reference
$\langle {}^{12}\mathrm{C} \vert {}^{14}\mathrm{C} \rangle_{0^+_1}$	0.66	−0.26	−0.69	This work
	0.66	−0.23	−0.25	Ref. [12]
	0.9	0.12	0.39	and [13]
$\langle {}^{12}\mathrm{C} \vert {}^{14}\mathrm{C} \rangle_{0^+_2}$	0.23	0.46	0.87	This work
	0.24	0.63	0.69	Ref. [12]
	0.43	0.46	0.75	and [13]
$\langle {}^{12}\mathrm{C} \vert {}^{14}\mathrm{C} \rangle_{1^-}$	$(p_{\frac{1}{2}})(s_{\frac{1}{2}})$	$(s_{\frac{1}{2}})(p_{\frac{1}{2}})$		
	0.9	0.9		
$\langle {}^{12}\mathrm{C} \vert {}^{14}\mathrm{C} \rangle_{3^-}$	$(p_{\frac{1}{2}})(d_{\frac{5}{2}})$	$(d_{\frac{5}{2}})(p_{\frac{1}{2}})$		
	0.7	0.9		

in table 2; similarly for the second step of the two-neutron transfer single-neutron overlaps of ^{5}He with ^{6}He and ^{13}C with ^{14}C are needed, the spectroscopic factors for these overlaps can also be found in the cited table 1.

The two-nucleon transfer will consist of a coherent superposition of three parts, the sequential single-nucleon transfer amplitudes, the one step amplitude for two-neutron transfer and the non-orthogonality term. The coherent sum gives the differential cross-section given by the relation

$$\sigma(\theta) = [f_{\mathrm{seq}}(\theta) + f_{\mathrm{1step}}(\theta) + f_{\mathrm{non}}(\theta)]^2 \,. \qquad (1)$$

Here the individual components of the two-nucleon overlap are directly determined by the spectroscopic amplitudes of the individual single-neutron transfer steps. For the unbound state of the $^5\mathrm{He}_{\mathrm{gs}}(p_{3/2})$ we have used the weakly bound approximation (with $E_B = 0.010$ MeV), because the angular-momentum barrier for $\ell = 1$ states produces a tail of the wave function which is rather independent of the binding energy, however, we use the correct asymptotic Q-values in the dynamical CRC calculation.

For the one-step two-nucleon wave function,

$$\Phi_{2n}(r_1, r_2)_{J^\pi} = \left\langle {}^{12}\,\mathrm{C}_{0^+} | {}^{14}\mathrm{C}\ {}_{J^\pi} \right\rangle ,$$

we subdivide the single-nucleon binding energy into equal halves. In this way a better asymptotic behaviour is achieved. However, we found that this procedure made only little difference as compared to the case where the product of the original two individual single wave functions are used. More relevant is the configuration mixing in the two-nucleon wave function $\Phi(1,2,R)$ which is represented by the following sum:

$$\Phi(1,2,R)_{0^+} \sim \sum_k a_k \left[\phi^k_{(nlj)}(R)\right]^2_{0^+} . \qquad (2)$$

Here the following definitions are used: $\phi^k_{(nlj)}$ is the single-particle wave functions, with the shell model quantum numbers (nlj); the coordinates r_1, r_2 are transformed into the R-coordinate which connects the centre of the two-nucleon wave function to the core. The mixing amplitudes a_k for the superposition of configurations in the 0^+ states are given in the table 2. The coefficients are obtained by multiplying the spectroscopic amplitudes of the first and second steps. For the negative-parity states usually only one configuration determines the structure:

$$\Phi(1,2,R)_{J^-} = [a_{1(nlj)} a_{2(nlj)} \phi^1_{(nlj)} \phi^2_{(nlj)}]_{J^-} , \qquad (3)$$

here again the product of the first and second step spectroscopic amplitudes are used. The same considerations are needed for the $\langle {}^6\mathrm{He} | {}^4\mathrm{He} \rangle$ two-neutron overlap, it has no configuration mixing in the present approach. We use the full $p_{3/2}$ strength without a $p_{1/2}$ admixture. Explicit calculations using the configuration mixing with the small $p_{1/2}$ shell admixture discussed in ref. [1] have been performed, but gave no distinct differences in the calculated result.

Due to the weak binding of the neutrons and the large difference in binding energies (positive Q-values) large non-locality effects for the ^{6}He systems are expected and various numerical tests have been made.

2.2 Numerical aspects of the CRC calculations

As in a previous study of one- and two-neutron transfer [14] induced by ^{11}Be on ^{12}C, numerical checks have been performed in order to asses the importance of various terms in the case of CRC-calculations with weakly bound systems. The second-order effects in single neutron transfer are very strong due to the large cross-sections.

The important parameters in the CRC calculation are, apart from the appropriate integration step length, the width and the range for the integration of the finite range integral. A test if these parameters are correctly chosen is obtained by comparing calculations in the prior and post representations. The results should not differ, however, for cases with very large Q-value (or angular-momentum mismatch), it becomes often difficult to achieve this independence. In this case the relevant recipes for reducing the non-orthogonality effects, known since more than 2 decades are used: the prior representation is used in the first step, and the post representation in the second/final step [11].

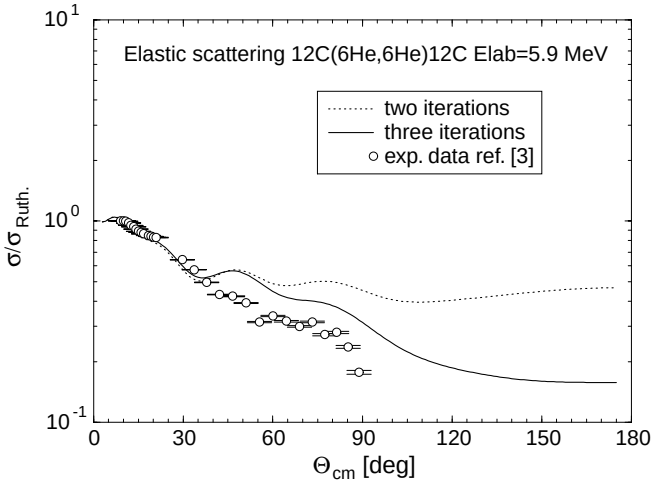

Fig. 2. Elastic scattering ^{6}He + ^{12}C at $E_{\mathrm{lab}} = 5.9$ MeV. The calculations are the result of using parameters in table 4.

We have also studied the dependence of the results on the number of iterations. There are big contributions of back coupling into the entrance channel. In order to obtain the sequential transfer two iterations are necessary, more iterations are needed to obtain a final convergence. In fig. 2 one can see the influence of higher order back coupling on the elastic scattering. We should note that the main part of this contribution comes from sequential one-neutron transfer processes, the contribution to the elastic scattering from the higher order two-neutron transfer process is small due to the comparably smaller probabilities for the population of the ^{14}C states. In the first calculation we used only second order coupling, because it turned out to be difficult to obtain convergence for small partial waves in calculations with higher iterations, due to the large couplings at small distances. In order to overcome this difficulty, we have used a strongly absorbing core of the imaginary potential, as in previous work [14], in order to damp couplings at small angular momenta and achieved convergence after more than 20 iterations. This result gives overall smaller absolute cross-sections, the real potential needs a very strong renormalisation for this case of strong coupling, a procedure, which has been discussed in the literature before [15]. Calculations with renormalised optical potentials and CFP-values are discussed in section 4.5.

For the other parameters of the calculations we cite the following values: due to the very long tails of the wave functions we had to use a maximum value of the radial integration limit of at least $R_{\max} = 35$ fm, similarly in order to come to a convergence of the values from calculations in the post or prior representations, the width of the nonlocal form factor had to be chosen larger than 6 fm.

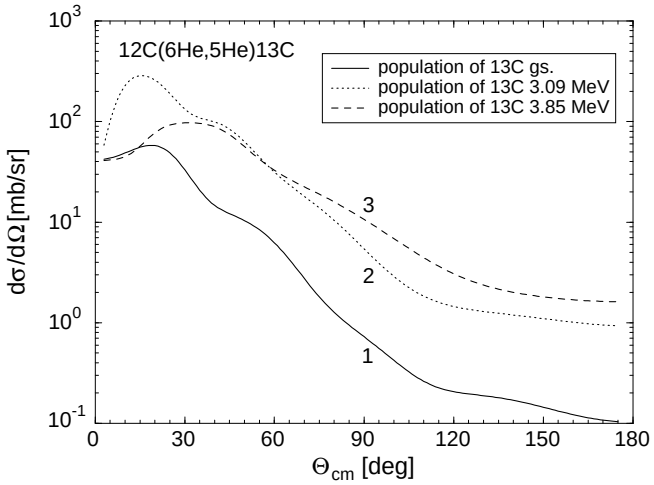

Fig. 3. Angular distributions of the one-neutron transfer cross-sections. Curves 1, 2, 3 correspond to the population of the states in ^{13}C g.s.($p_{1/2}$), 3.09 MeV($s_{1/2}$), 3.85 MeV($d_{5/2}$).

3 Structure aspects of the reaction ^{6}He+^{12}C

3.1 Wave functions of ^{13}C and ^{14}C

The structure of the low-lying states of ^{13}C and ^{14}C is well known [16], the spectroscopic amplitudes for the $p_{1/2}$, $s_{1/2}$ and $d_{5/2}$ shells have been determined repeatedly and values are compiled in table 1 and 2 , where we show the relevant information for the values of this work. For the one-step 2n-transfer the product of the single one-neutron transfer amplitudes are directly used. Note, however, that special two-neutron wave functions are cited [12,13] with the amplitudes for the individual configurations directly taken from the literature. In one case (ref. [12]) a negative sign is given to the *sd*-shell amplitudes for the ground state (0^+), and a positive sign for the excited 0^+ state; this feature represents the collective pairing property of the ground state. Its consequences are well seen in the results of the calculation, where the sequential and one-step amplitudes are added coherently (see figs. 4, 5). For the negative parity states only one configuration is used, however, two different sequential routes (and amplitudes) contribute as indicated in fig. 1 by the dashed lines for the 3^--state.

3.2 Wave functions of ^{5}He and ^{6}He

The structure of ^{6}He has been the subject of numerous studies because the subsystems ^{5}He and the two neutrons are not bound. A complicated spatial distribution of the wave functions has been predicted [1]. The part of the wave function which corresponds to a "di-neutron" extends to the surface of ^{6}He, we expect that this part will dominantly contribute to the two-neutron reaction at the low-energy considered here. The dominance of the contributions of the "di-neutron" has also been observed in ref. [2] at much higher energy.

Table 3. Binding potentials for neutron bound states in He and carbon.

	V (MeV)	r (fm)	a (fm)	V_{ls} (MeV)	r_{ls} (fm)	a_{ls} (fm)
^{12}C+n	−46.8	1.20	0.9	7.0	1.20	0.9
^{13}C+n	−54.08	1.20	0.9	7.0	1.20	0.9
^{5}He+n	−52.6	1.20	0.9	7.0	1.20	0.9
^{4}He+n	−51.15	1.20	0.9	7.0	1.20	0.9
	Gaussian shape					
^{5}He+n	−61.05	$b = 2.3$		7.0	1.20	0.9
^{4}He+n	−56.11	$b = 2.3$		7.0	1.20	0.9

Table 4. Optical potentials [17,18].

Potentials	V (MeV)	r (fm)	a (fm)	W (MeV)	r_w (fm)	a_w (fm)
^{6}He+^{12}C	−46.15	0.91	0.57	−25.0	0.6	1.43
ref.[17]						
CRC	−96.0	0.91	0.57	−10.0	1.1	0.5
ref.[18]	−177.0	1.3	0.57	−12.0	1.5	0.6
^{5}He+^{13}C	−46.15	0.91	0.57	−25.0	0.6	1.43
		same	values			
^{4}He+^{14}C		same	values			0.7

For the present reaction at the moderate energy of $E_{\rm lab}$ = 5.9 MeV a typical surface stripping process, as often observed with heavy ions [7] is expected to occur. Therefore we will use a rather simple model of ^{6}He with a $(p_{3/2})^2$ configuration, as reflected in the spectroscopic factors chosen, which are 1.0 and 2.0 for the first and second neutron, respectively. There is still an ambiguity with the Q-value of the intermediate step: we use the correct Q-value of the ^{5}He-channel, but we use a quasi-bound approximation for the ^{5}He ground state with a binding energy of 0.01 MeV. This approximation seems to be rather good in view of the dominance of the $\ell = 1$ centrifugal barrier of the $p_{3/2}$ configuration. For the two-neutron wave function we use the correct asymptotic binding energy of 0.98 MeV.

Calculations of the sequential process, where the ^{5}He state is treated as a resonance have also been made using the FRESCO code [11], however, the difference to calculations with the quasibound approximation are to small, to be considered in this discussion. As we will see later, the sequential two-step 2n-transfer dominates the transitions to the odd-parity states and for the 0^+ states it also contributes at least 50%.

3.3 Bound-state potentials

In the analysis we have to choose the bound-state potential for the quasibound states in ^{5}He and the bound state in the $\langle {}^{5}\mathrm{He}|{}^{6}\mathrm{He}\rangle$ channel. The parameters of the binding potentials for the helium nuclei and for the description of the bound states in ^{13}C and ^{14}C are indicated in table 3. The relevant values for the central (Woods-Saxon shape) and the spin orbit potentials are given.

For the $^{5-6}$He wave functions we have also used the Gaussian-shape of the binding potential as in ref. [1].

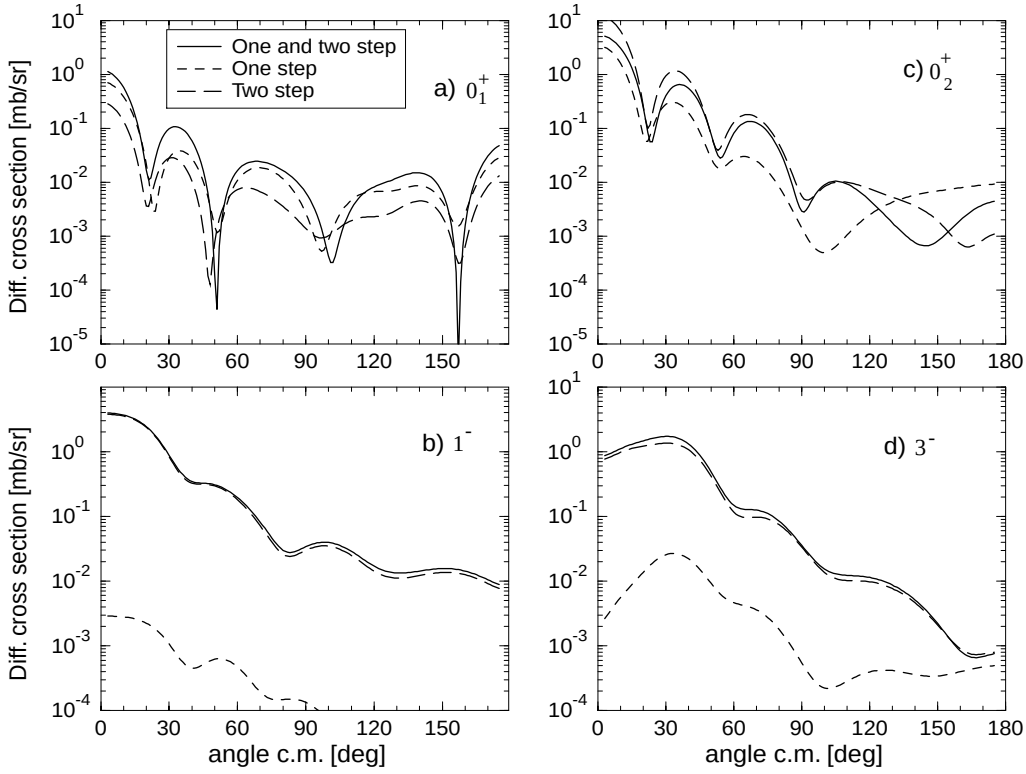

Fig. 4. Results of the second-order calculations for the differential cross-sections for the reaction,^{6}He + ^{12}C $\rightarrow^6$He + ^{14}C at E_{lab} = 5.9 MeV : a) – $^{14}C_{gs}$, b) – $^{14}C^*_{1^-}$, 6.09 MeV, c) – $^{14}C^*_{0^+_2}$, 6.59 MeV, d) – $^{14}C^*_{3^-}$, 6.73 MeV.

This choice actually produced a slightly higher 2n-transfer cross-section relative to Woods-Saxon (WS) potentials given in the table, by 20% in the first maximum and factor 2 in the secondary maximum at 30° (see figs. 7 and 8). The RMS radius of ^{6}He, which corresponds to the chosen binding potentials is 2.35, for a radius parameter $r = 1.2$ fm and the diffuseness of $a = 0.9$ fm; taking a radius parameter of 1.9 fm increases the RMS radius to 2.45 fm. For the Gaussian shape of the potential we have RMS = 2.21 fm (for a Gaussian width of 2.3 fm). For the RMS radius of ^{4}He which enters into this discussion, a value of RMS = 1.47 fm is used. We varied the binding potentials for the neutron bound states in order to obtain different RMS radii, as discussed in section 4 the influence on the differential cross-section is small and *larger RMS produced smaller differential cross-sections* at angles smaller than 90°.

4 Results of CRC calculations

4.1 Optical potential parameters

Another important ingredient for the CRC-calculation is the scattering potential for the ^{6}He elastic channel and the exit ^{4}He channels. We have chosen two different parameter sets given in table 4, one which reproduces very precisely the phase shifts of low energy α-^{12}C scattering [17], and another set which reproduces well the background (potential) scattering at higher energies [18]. In addition table 4 gives parameters used in a full CRC calculation (25 iterations and increased CFP values) discussed below in section 4.5.

The first potential is moderately attractive and gave rather good description of the elastic scattering with an adequately chosen imaginary potential. Actually, due to the large cross-section for single neutron transfer the explicit coupling of the transfer channels introduces a sizable effect on the elastic channel as illustrated in fig. 2. However, this potential fails if higher order couplings are calculated, due to very strong couplings at small distances and no convergence is observed. We have chosen a large diffuseness for the imaginary potential for the ^{6}He and ^{5}He channels in order to describe the absorption at large angles due to break-up (or transfer to the continuum), which we have not considered in these calculations.

The second choice of potentials from higher energy α-scattering is strongly refractive. With these potentials the elastic scattering can be well reproduced, however, the 2n-transfer cross-section obtained are more than a factor 10 smaller than in the other case. These calculations are not shown, we think that these potentials are much to deep for our case at low energy. It is actually known, that the study of transfer channels can help to reduce the ambiguities in optical model potentials [7].

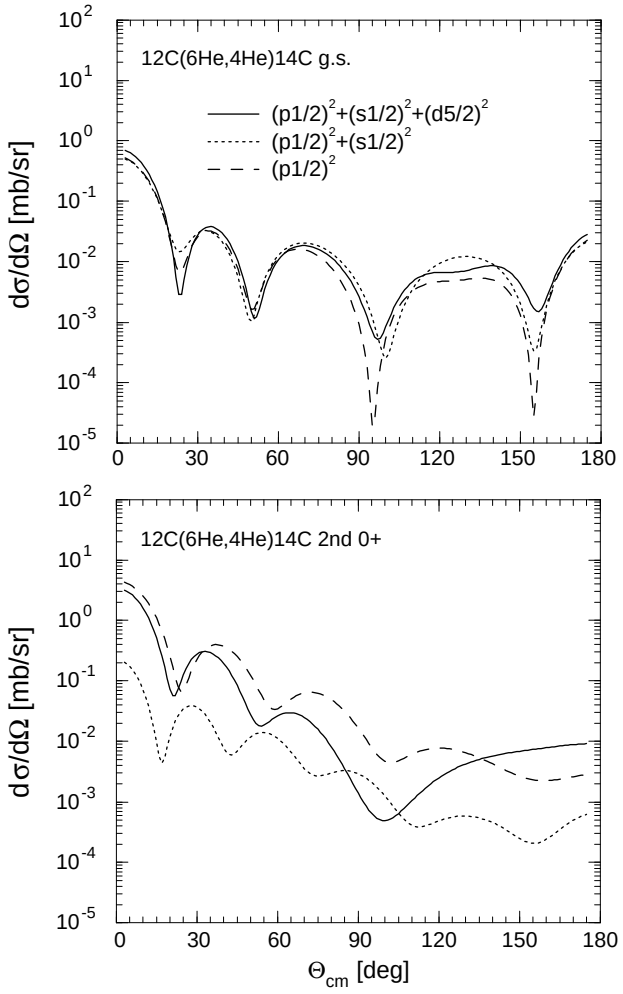

Fig. 5. Results of second-order calculations for the 0^+ states populated in the *one-step* transfer processes with various degrees of configuration mixing in the wave functions of ^{14}C as given in table 2.

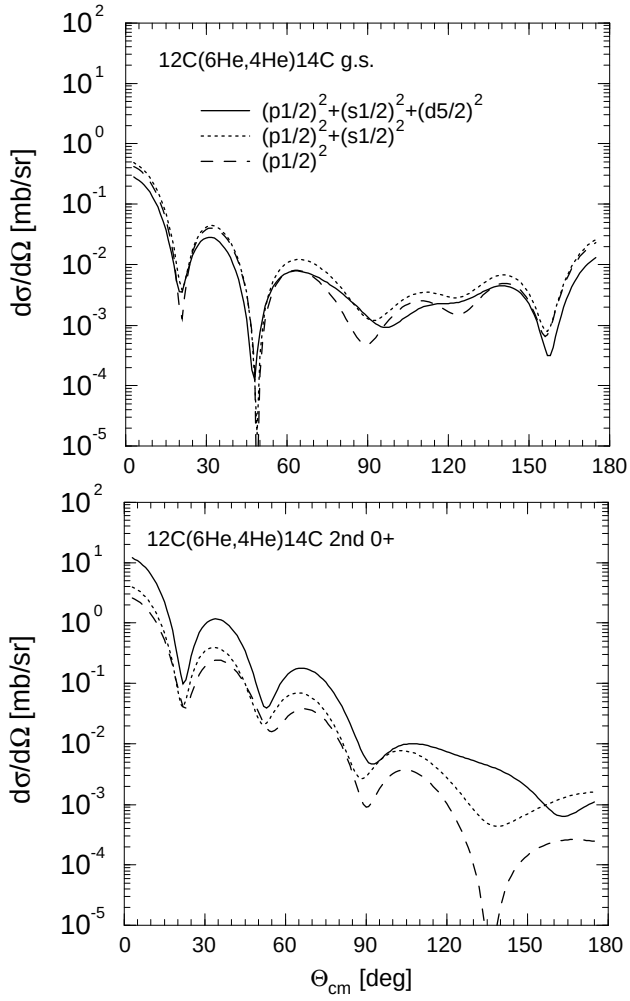

Fig. 6. Results of second-order calculations for the 0^+ states populated in the *two-step* transfer processes with various degrees of configuration mixing in the wave functions of ^{14}C as given in table 2.

In the exit channel for ^{4}He+^{14}C the diffuseness of the imaginary potential has been reduced to a value of 0.7 fm. As in previous calculations we have used a core absorptive potential ($W_0 = 20$ MeV, $r_w = 0.5$ fm, $a_w = 0.3$ fm) in order to facilitate the convergence of the CRC calculations which tend to show strong coupling at very small distances. For the results which include inelastic excitation of ^{6}He (2^+) state and full CRC coupling (about 25 iterations) we have used an even more absorptive core ($W_0 = 80$ MeV, $r_w = 0.5$ fm, $a_w = 0.25$ fm). The results for the one-neutron transfer are shown in fig. 3, the results in the second-order CRC are compiled in figs. 4–8. The result of the full CRC calculation is shown in fig. 9.

4.2 One- and two-step neutron transfer

As mentioned in the introduction the transfer of two neutrons will contain three terms, the one-step, the sequential transfer and the non-orthogonality term. In fig.4 we show for each of the four states in ^{14}C the result of the calculations for the individual contributions and for the sum. For the ground state (0^+) we notice a slight dominance of the one-step contribution and a constructive interference between the one- and two-step amplitudes. For the excited 0^+-state the sequential transfer dominates, the one-step amplitude introduces a destructive interference of the two amplitudes. For the negative-parity states with spin parity (1^-) and (3^-)—as expected—the sequential transfer dominates by factors 100–1000, implying that there is no "di-neutron" structure involved in this transfer process.

The different configurations responsible for this behaviour have been mentioned before and the effect of configuration mixing is discussed in more detail in the next section.

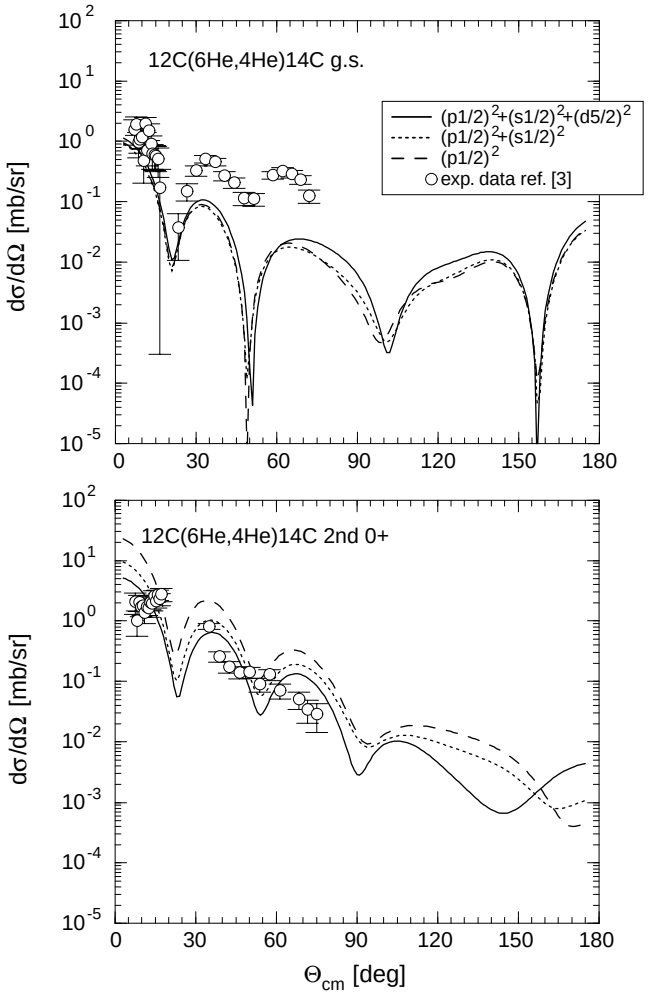

Fig. 7. Results of second-order calculations for the 0^+ states populated in the *one- and two-step* neutron transfer processes with various degrees of configuration mixing in the wave functions of ^{14}C as given in table 2.

4.3 Configuration mixing

Whereas for the ^{6}He wave function we have used the pure $(p_{3/2})^2$ wave function, it is necessary to consider configuration mixing to the 0^+ states in ^{14}C. A particularly interesting case of configuration mixing is realized in these 0^+ states. The ground state (and the excited 0^+ state) will consist of amplitudes of the *p*-shell and *sd*-shell, both acting constructively in the ground state (this is realised by a negative sign of the *sd*-shell amplitudes shown in table 2).

We can follow the build-up of the cross-section in the case of sequential and one-step transfer in figs. 4, 5, 6 and 7. We see that the addition of *s*- and *d*-shell amplitudes give an increase in the cross-section in particular for the two-step process. This phenomenon of mixing of two different shells with opposite parity, known from previous work, is also responsible for the large spatial extension of the di-neutron in ^{11}Li as discussed in several refs. [1, 13]. We note that the signs of the two neutron amplitudes which are chosen in this work in accordance with those proposed in ref. [12] give particular behaviours: i) the destructive and constructive effects in figs. 5 and 6, favouring the excited 0^+ state; ii) the constructive (destructive) interference of the one-step and two-step amplitudes in the GS (0^+) and excited (0^+) states, respectively.

4.4 Dependence of the cross-section on RMS radii and final result

It is well known that the absolute cross-sections depend on the parameters of the potential used to create the binding states. This occurs through the differences of the tails of the wave functions and through the potential itself, which enters as the effective interaction of the transfer process. In the present case we looked into the dependence of the cross-sections on the root mean square radius (RMS) by varying the binding potential parameters.

For the weakly bound system like ^{6}He the values of the RMS-radius (see [1]) are often used to discuss the radial extension of the wave function and its relation to break-up cross-sections is cited. Actually the total reaction cross-section of ^{6}He (dominated by break-up processes) is used and an experimental value of $R_{\rm exp}$(RMS ^{6}He)=2.57± 0.1 fm is cited in ref. [1]. We have looked into the dependence of the two-neutron transfer reaction cross-section on the value of RMS of ^{6}He. We found that the 2n-transfer cross-section *decreased* by 20% if the RMS is *increased* from 2.35 fm to 2.46 fm. This effect may be understood, because we observe a strongly structured angular distribution for the 0^+ states, which is due to large far-side contributions to the amplitudes originating from the nuclear interior (due to the refractive optical potential). These far-side contributions sample the nuclear wave function inside of the Coulomb barrier and inside of the "interaction" radius. A larger RMS radius (obtained with a smaller radius of the binding potential) corresponds to smaller values of the wave function at small distances. The two-neutron transfer reaction thus samples completely different parts of the 2n-wave functions as compared to the total reaction cross-section used to deduce the $R_{\rm exp}$(RMS)-value cited above. We keep the values of the binding potential as cited in table 3. for our final comparison with the data.

For a final comparison (shown in fig. 8) we use the Gaussian shape of the binding potential for ^{6}He and a reduced value (compared to table 4) of the imaginary part of the α+^{14}C-channel (W = 10 MeV, r_w = 1.2 fm a_w = 0.7 fm). We see that the absolute cross-section of all four states are reasonably well described with the choice of the present parameters. Some deficiencies of the calculations appear for the second and third maximum of the 0^+ states. This may be related to an incomplete description of the contribution from small distances, which could be related to some components of the ^{6}He wave functions, or more likely, to some details of the optical potential parameters and higher order couplings (compare next subsection). However, we consider the result for the shape of the angular distributions and the overall agreement in absolute cross-section as rather satisfactory.

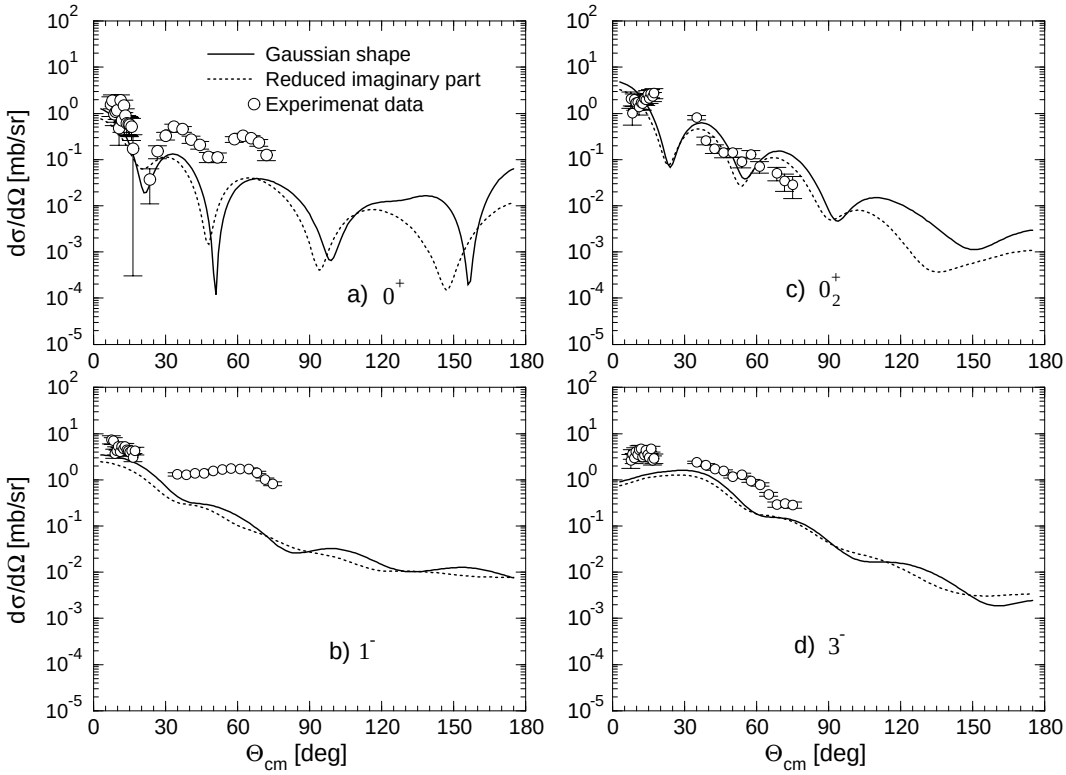

Fig. 8. Final result of the second-order calculations for the ^{12}C(^{6}He,^{4}He)^{14}C reaction using a Gaussian shape of the binding potential in $^{5-6}$He and two versions of the imaginary potential.

4.5 Full CRC results

In the present reaction a strong coupling occurs if we follow the iterations beyond second or third order. In fact these higher order couplings are needed to describe the experimental data correctly. However, with the introduction of the full coupling the calculated absolute cross-section drops by a factor 5–10 (see in fig. 9 the curve labelled "normal"). To get an improvement in the value of absolute cross-sections in the full CRC calculation we have to increase the strength of coupling by about 70%. In fig. 9 the results for the full CRC (25 iterations) calculations are shown. The full curve corresponds to the normal strength of coupling and the dotted one to the increased strength (which is only done in the (^{6}He/^{5}He/^{4}He)-branch (CFP(2n)=3.4, CFP$_1$(1n)=1.7, CFP$_2$(1n)=2.0).

In the full CRC case a considerable renormalisation of the optical potential is needed. In the frame of Feshbach's formalism the optical potential may be written as ref. [15] (here V_{00} is a "bare"-potential),

$$U_{\rm opt} = V_{00} + \Delta V\,, \tag{4}$$

where

$$\Delta V = \sum_{\alpha\alpha'} V_{0\alpha} \left(\frac{1}{E - H - i\varepsilon}\right)_{\alpha\alpha'} V_{\alpha'0}\,,$$

and ΔV is the so called dynamical polarisation potential (DP) which arises due to coupling from the elastic channel "0" to all channels α, α'

As was shown in the previous sections we have a rather good description of the differential and absolute cross-sections in second-order approach with optical model parameters cited in table 4. Now, in the case of full CRC approach, due to strong coupling to the channels the influence of DP potentials starts to play an essential role. We used renormalised parameters of optical potentials listed in table 4 as "CRC". We note that the real potential has to become much deeper. This corresponds to the observation in other reactions discussed by Sakuragi [15], where the coupling introduces a repulsive effect, if described by the local potential.

In fig. 9 the final results for the full CRC calculations are shown. There we illustrate the results with normal and increased strengths (full and dotted curves). We note that the calculation shows more pronounced structure in the case of the second (0^+_2). It could be possible that the data have here a systematic problem because of limited resolution in separating the 0^+_2 and 3^- states. We have also studied the influence of the "indirect" routes via the inelastic excitation of ^{6}He (2^+) state. This is done by treating the 2^+ in a deformed collective model with a deformation parameter (β_2=0.73) as reported by Aumann *et al.* [20] ($B(E2; 0^+ \to 2^+)$=3.2 e^2fm^4, we use r_c=1.25 fm). The dashed curve corresponds to $\beta_2 > 0$ and dot-dashed to the negative sign of β_2. One can see, that the influence of the ^{6}He (2^+) channel is not very large as can be expected because of the small cross-section of the 2^+ state

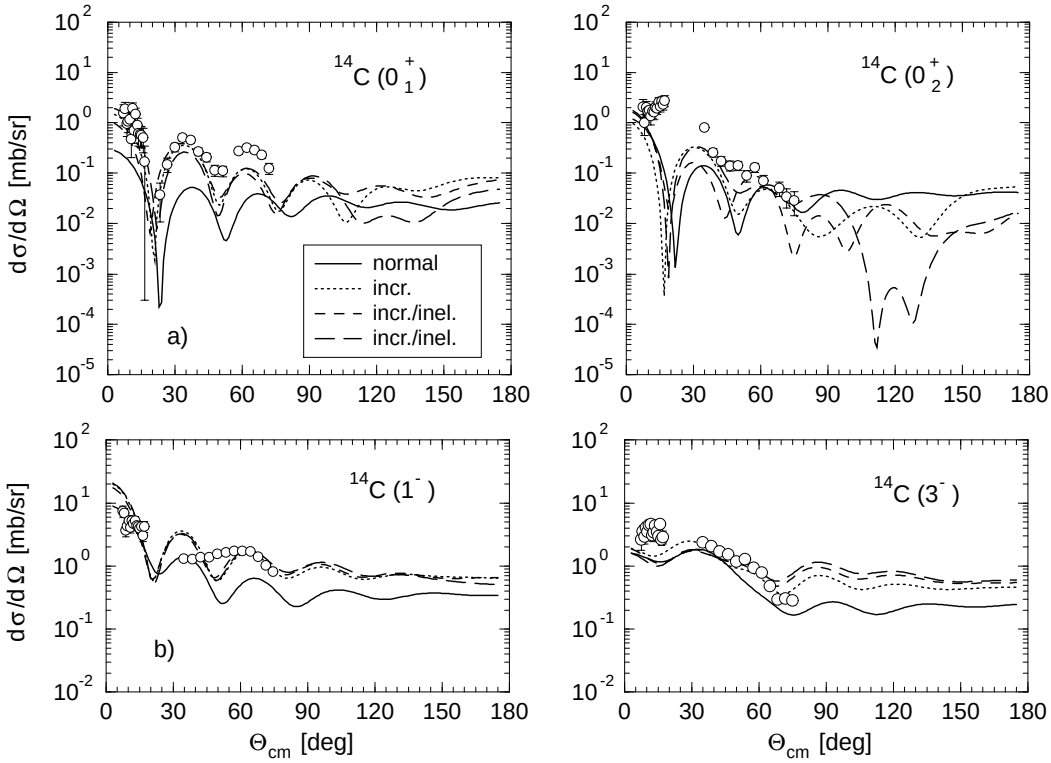

Fig. 9. Full CRC calculation for the ^{12}C(^{6}He,^{4}He)^{14}C reaction with 25 iterations leading to states in ^{14}C as in fig. 8. The curves are labelled for different choices of spectroscopic amplitudes and couplings as explained in the text.

(the calculated total cross-section for inelastic excitation of ^{6}He (2^+) is approximately 49 mb).

5 Conclusions

In this work we have obtained a satisfactory description of the two-neutron transfer cross-sections induced by ^{6}He on ^{12}C at a low energy of $E_{\rm lab} = 5.6$ MeV. In the second-order calculation the absolute cross-section for the 0^+ states are typically under predicted by a factor two. This discrepancy could possibly be removed by a more detailed search of potential parameters, which could have been varied in the exit channel more extensively. In the present analysis we observe that the differential cross-sections for odd-parity states are well described (also the absolute values) by a sequential neutron transfer process, whereas for the 0^+ states a complicated interference of amplitudes with different configurations in the one and two-step processes occurs.

The dependence of the cross-section on the root mean square (RMS) radius of ^{6}He has been studied; it has been found that the differential cross-section decreased for increasing RMS values. This effect may be attributed to the occurrence of large refractive far-side contributions in two-neutron transfer to the differential cross-section at small angles, which in fact show very pronounced structures. The reaction thus samples a larger part of the wave function which extends to the nuclear interior. This effect in heavy-ion–induced two-nucleon transfer has actually also been shown in ref. [7]. The various spectroscopic amplitudes used in the present analysis were mostly known from the literature, and were slightly adjusted. Due to the large amplitudes of the neutron wave functions higher-order coupling calculations (CRC) have been performed. In these cases the spectroscopic amplitudes of ^{6}He and the parameters of the optical model had to be renormalised. The final result was an improved fit of the shapes of the angular distributions. The indirect route via the ^{6}He (2^+) state was found to be of minor importance. We conclude that due to the many parameters entering into the final result it does not seem to be possible to make a detailed study of the ^{6}He wave function from two-neutron transfer studies.

This work has been partially supported by funds of The Federal Ministry(BMBF-Verbundforschung-FOBOS). We are indebted to Wilfried Galster and A.Piechaczek for making the data available to us.

References

1. M.V. Zhukov, B.V. Danilin, D.V. Fedorov *et al.*, Phys. Rep. **231**, 151 (1993).
2. Yu.Ts. Oganessian, V.I. Zagrebaev, J.S. Vaagen, Phys. Rev. Lett. **82**, 4996 (1999).
3. A.N. Ostrowski, A.C. Shotter,W. Bradfield-Smith et al., J. Phys. G **24**, 1553 (1998).

4. R. Wolski, A S. Fomichev, A.M. Rodin et al., Phys. Lett. B **467**, 8 (1999).
5. G.M. Ter-Akopian et al., Phys. Lett. B **426**, 251 (1998).
6. R. Raabe, A. Piechaczek, A. Andreyev et al., Phys. Lett. B **458**, 1 (1999).
7. R.J. Asciutto, and E. Seglie, in *Treatise on Heavy Ion Science*, edited by D.A. Bromley, Vol. **1** (Plenum Press, New York, 1984) p. 463.
8. B.F. Bayman, J. Chen, Phys. Rev. C **26**, 1509 (1982).
9. M. Igarashi, K.I. Kubo Phys. Rep. **199**, 1 (1991).
10. Th.Wilpert, B. Gebauer, M. Wilpert et al., Z. Phys. A **358**, 395 (1997).
11. Ian J. Thompson, Computer Phys. Rep. **7**, 167 (1988).
12. H.T. Fortune, G.S. Stephans, Phys. Rev. C **25**, 1 (1982).
13. N. Vinh Mau, J.C. Pacheco, Nucl. Phys. A **607**, 163 (1996).
14. I.V. Krouglov, Thesis, St. Petersburg State University, 1998; see also W. von Oertzen and I. Krouglov, Phys. Rev. C **53**, R1061 (1996),
15. Y. Sakuragi et al., Prog. Theor. Phys. Suppl. No. 89 (1986).
16. F. Ajzenberg-Selove, Nucl. Phys. A **523**, 1 (1991); Nucl. Phys. A **449**, 1 (1986).
17. H. Oeschler, H.Fuchs, H.Schröter, Nucl. Phys. A **202**, 513 (1973).
18. R. Plaga et al., Nucl. Phys. A **465** (1987).
19. M. Yasue et al., Nucl. Phys. A **509**, 141 (1990).
20. T. Aumann et al., Phys. Rev. C **59**, 1252 (1999).